CLM-P890

CLM-P890

First measurements of the particle confinement in a Reversed Field Pinch by the laser ablation method

P. G. Carolan
A. Patel
M. C. Sexton
M. J. Walsh

CULHAM
LABORATORY

AEA TECHNOLOGY

First measurements of the particle confinement in a Reversed Field Pinch by the laser ablation method

P. G. Carolan, A. Patel, M. C. Sexton* and M. J. Walsh*†

Culham Laboratory, Abingdon, Oxon, OX14 3DB, United Kingdom

(Euratom/UKAEA Fusion Association)

Abstract

We report the first use of laser ablation of trace impurities into a Reversed Field Pinch, similar to that used on Tokamaks, but selecting different impurity elements appropriate to the confinement times of present RFPs. Ionisation rates from helium-like carbon and boron are sufficiently slow to allow measurements of the particle confinement time from line intensity decay rates of the near UV transitions. A zero dimensional treatment, incorporating impurity ionisation and confinement, is used to interpret the temporal behaviour of the line intensity. The results obtained yield typical particle confinement times of about 1ms.

---

*University College Cork, Ireland.

†Supported by a grant from EURATOM.

Hitherto, investigations of particle transport in Reversed Field Pinches, relied on the presence of intrinsic impurities, such as carbon and oxygen [1]. This method of determining the impurity transport requires absolutely calibrated spectrometers and spatially resolved measurements (e.g. electron temperature, T_e, and density, n_e), and is dependent on the parameter profiles used (e.g. flat or hollow diffusion coefficient spatial distribution).

A more direct method of measuring particle confinement, or transport, involves the laser ablation [2] of trace quantities of an appropriate impurity (e.g. iron, nickel for Tokamaks) [3,4] into a plasma and monitoring the line-radiation time histories. In using this method, the ablated impurities that are suitable to the plasma parameters in RFPs have to be determined.

Although the electron temperatures and densities in present RFP plasmas are typical of similar sized Tokamaks, the diffusion coefficient is much larger ($\langle D\rangle \approx 100 \mathrm{m^2 s^{-1}}$ for RFPs [1] compared with typically $\langle D\rangle \approx 1 \mathrm{m^2 s^{-1}}$ for Tokamaks e.g. ref [5]) so that the impurities are at considerably lower ionisation states. The expected range of $n_e\tau_p$ ($\approx 0.1\text{–}1 \times 10^{16} \mathrm{m^{-3}s}$, where τ_p is the impurity particle confinement time) and T_e ($\approx$ 200–500eV) in RFPs ensures that even helium-like ionisation states are not fully burnt-through for low-Z elements, like carbon and oxygen, before the impurities are lost from the plasma [6].

The selection of suitable ablated impurities depends on several factors: (i) the ionisation state of interest should reside in the plasma core (ii) the emitted spectral lines should lie in the range accessible to our spectrometers (600–10000Å) and (iii) the spectral line intensity should be sufficiently bright to avoid the use of large levels of injected material. The first two conditions are satisfied by the helium-like states of the elements boron to fluorine which have sufficiently long ionisation times to the hydrogen-like states and where the existence of the meta-stable level ($1s2s\,^3S$) also allows near UV transitions ($1s2s\,^3S$–$1s2p\,^3P$). However, the photon emission rate for this transition decreases sharply with increasing atomic number. This can be seen from the results of calculations for these elements from available

ionisation cross-sections [7,8], excitation rates [9] and spontaneous decay probability coefficients [10] as summarised in Table I. The use of boron and carbon avoids the necessity of using compounds of ablation material which is required for nitrogen, oxygen and fluorine.

In the HBTX1C RFP [11], the carbon concentration is typically a few percent of n_e, hence the injected concentration must be at least of this order but not so high that the plasma is perturbed (e.g. less than $\approx 10\%$ change in n_e or in the radiated power). Boron injection does not have this difficulty since it is not an intrinsic impurity, but it has the disadvantage of having a shorter ionisation time from the helium-like state, BIV. This means that the line intensity behaviour is less sensitively dependent on the particle confinement time.

These elements were evaporated onto a 3mm thick glass target-disk, 50mm in diameter. Using a 300–400Å layer of chromium as an intermediary, coatings of thickness 3μm and 1μm were laid for carbon and boron, respectively. For a laser beam waist of 2mm at the target, these thicknesses correspond to a few times 10^{17} atoms injected into the plasma ($\approx 1\text{m}^3$ volume). In practice, the laser power and beam waist were adjusted so as to optimise the detected line intensity while restricting the measured increase in n_e, following ablation, to $\leq 10\%$.

The apparatus used to launch the particles is shown schematically in figure 1. The system consists of a 3J, Q-switched ruby laser, a moveable lens and an iris to allow the spot size and energy density to be varied. The CV and BIV emissions (with wavelengths 2270.9Å, 2277.2Å, 2277.96Å and 2821.7Å, 2824.6Å, 2825.86Å, respectively) are monitored using a polychromator [12], and a visible spectrometer which are respectively located 180° and 90° toroidally from the ablation port. Typical temporal behaviour of the line intensities from carbon and boron are shown in figure 2. The waveforms have the similar characteristics of (i) a short rise time, and (ii) an exponential decay to the pre-ablation level. The former indicates rapid burn-through of the lower ionisation states, until the helium-like state is

reached, and the fast transport of the impurities from the ablation port location to the viewing chords of spectrometers.

Here we are more interested in the line intensity decay rate and how this relates to the particle confinement time. We have constructed a simple zero dimensional model which treats the ionisation and loss of impurities. The rate equation for the k^{th} ionisation state is described by:

$$\frac{\mathrm{d}n_k}{\mathrm{d}t} = n_e S_{k-1} n_{k-1} - n_e S_k n_k - \frac{n_k}{\tau_p} \tag{1}$$

where

$n_k \equiv$ impurity density of the k^{th} ionisation stage

$S_k \equiv$ ionisation rate coefficient from state k to $k+1$

and $\tau_p \equiv$ particle confinement time (assumed the same for all states)

Conditions in the HBTX series of experiments are such that impurity states are far from coronal equilibrium ($n_e\tau_p \approx 1\text{–}2\times10^{18}\mathrm{m}^{-3}\mathrm{s}$), and, consequently, recombination is relatively slow and is neglected in equation 1. The recycling of ablated materials is also negligible as was observed from having alternate discharges with and without laser ablation. Therefore, equation 1 is sufficiently representative of the impurity ionisation and loss in this zero dimensional treatment. The system of equations generated from equation 1 are then solved analytically. Sample simulations of the evolution of the carbon ionisation stages are shown in figure 3 for n_e of $1.5\times10^{19}\mathrm{m}^{-3}$ and T_e=200eV. In the decay phase, it can be seen that the lithium-like state is relatively unpopulated, thus giving:

$$\frac{\mathrm{d}n}{\mathrm{d}t} \approx -n_e S n - \frac{n}{\tau_p} \tag{2}$$

$$\Rightarrow n \propto \exp\left[-\left(S n_e + \frac{1}{\tau_p}\right) t\right] = \exp\left[-\frac{t}{\tau_m}\right] \tag{3}$$

where n represents the density of helium-like impurities, S is the ionisation rate coefficient to the hydrogen-like state and τ_m is the measured decay rate. Thus, the particle confinement time can be unfolded from the raw data with relative ease once n_e and T_e are known. It should be

noted that (i) the accuracy of the result increases with decreasing particle confinement time, and (ii) the directly measured decay time, τ_m, of the line intensity gives the lower limit of τ_p. The experimental data for carbon in figure 2 yields τ_m=0.63±0.06ms. Using equation 3 and an ionisation time, $1/Sn_e$, of 1.6±0.4ms (T_e=200±30eV, n_e=(1.5±0.15)×10^{19}m^{-3}), we get τ_p=1.0ms$^{+0.7ms}_{-0.1ms}$. From the boron results we obtain τ_m=0.4±0.1ms. By applying the same analysis as previously and incorporating the ionisation time 0.55±0.15ms (T_e=200±30eV, n_e=(1.1±0.11)×10^{19}m^{-3}), we get a lower limit of $\tau_p \approx$1.2ms. The lower limit to the ionisation time is too short to allow a realistic upper limit to τ_p to be obtained. Implicit in the foregoing is that the BIV ionisation state resides in the plasma centre (i.e. at maximum T_e and n_e values). This is unlikely and in practice the contributions to the line intensity will be dominated by the off-centre region where the lower ionisation rate will ensure a higher BIV concentration. However, without more detailed data and analysis (e.g. one dimensional treatment), we prefer to quote the lower limit only of τ_p=1.2ms which supports the carbon results.

By assuming that the particle flux across the fields in the centre of the machine is dominated by radial diffusion, we can evaluate a relationship between the diffusion constant and the particle-confinement-time [13] on axis. Choosing a parabolic density profile, this is given by

$$\tau_p = \frac{a^2}{4D_{axis}} \tag{4}$$

where a (0.255m) is the minor radius of the plasma. Using a τ_p of 1.0ms, this yields an on-axis diffusion coefficient of $\approx$15m^{2}s^{-1}. This corroborates previous estimates based on ion power balance considerations [13].

To conclude, we have shown that laser ablation of low-Z impurities can be usefully applied to the study of transport in Reverse Field Pinch plasmas. Particle confinement times of about 1ms are obtained in the HBTX1C experiment at typical conditions of 100kA plasma current and T_e=200eV, and n_e=1.5×10^{19}m^{-3}.

Acknowledgements

The authors acknowledge the technical support provided by the HBTX team. Special thanks go to M. J. Butler, T. J. Dodd and J. K. Fletcher.

References

[1] P. G. Carolan, C. A. Bunting, A. M. Manley, A. Patel, Proc. EPS, 14^{th} European Conf. on Controlled Fusion and Plasma Physics(Madrid), II, 515, (1987).

[2] J. F. Friichtenicht, Rev. Sci. Instrum., **45**, 51, (1974).

[3] E. S. Marmar, J. L. Cechi, S. A. Cohen, Rev. Sci. Instrum., **46**, 1149, (1975).

[4] C. Breton *et al,* "Low energy neutral beam production by laser vaporisation of metals", EUR-CEA-FC-1015, (1979).

[5] K. H. Behringer, P. G. Carolan *et al.*, Nuclear Fusion, **26**, 751, (1986).

[6] P. G. Carolan, V. A. Piotrowicz, Plasma Physics, **25**, 1065, (1983).

[7] K. L. Bell, H. B. Gilbody, J. G. Hughes, A. E. Kingston, F. J. Smith, "Atomic and molecular data for fusion, part 1", Culham report CLM-R-216, (1981).

[8] M. A. Lennon, K. L. Bell, H. B. Gilbody, J. G. Hughes, A. E. Kingston, M. J. Murray, F. J. Smith, "Atomic and molecular data for fusion, part 2", Culham report CLM-R-270, 1986.

[9] Y. Itikawa, S. Hara, T. Kato, S. Nakazaki, M. S. Pindzola, D. H. Crandall, "Recommended data on excitation of carbon and oxygen ions by electron collisions", IPPJ-AM-27, (1983).

[10] W. L. Wiese, M. W. Smith, B. M. Glennon, "Atomic transition probabilities, hydrogen through neon", Publishers: National Bureau of Standards, (1966).

[11] B. Alper, M. K. Bevir, H. A. B. Bodin *et al.*, Proc. EPS, 16^{th} European conf. on Controlled Fusion and Plasma Physics(Venice), II, 705, (1989).

[12] P. G. Carolan and A. Patel, Rev. Sci. Instrum., **57**, 552, (1986).

[13] P. G. Carolan, A. Lazaros, M. G. Rushbridge, J. W. Long, "Ion heating and power balance in the reversed field pinch", Culham report CLM-P-852 (1989), submitted to physical review A.

Element	τ_i ms	Fractional abundance of helium-like	Fractional population of $1s2p^3P$ level	A values for $1s2s^3S$–$1s2p^3P$ $10^8 s^{-1}$	No. of photons emitted ph./ion/sec
Boron	0.4	0.1	2×10^{-4}	0.455	9100
Carbon	1.6	0.6	6×10^{-5}	0.565	3390
Nitrogen	7	0.8	1.5×10^{-5}	0.678	1017
Oxygen	33	0.9	3×10^{-6}	0.794	238
Fluorine	161	0.9	7×10^{-7}	0.915	64

Table I: *Parameters of interest in selecting appropriate elements for ablation at T_e=200eV and n_e=1.5×10^{19}m^{-3}. The ionisation time, τ_i, is that from the helium-like to hydrogen-like states. The fractional abundances are calculated at 1ms following impurity injection. Note that the fractional population of the $1s2p^3P$ level is estimated for boron and fluorine.*

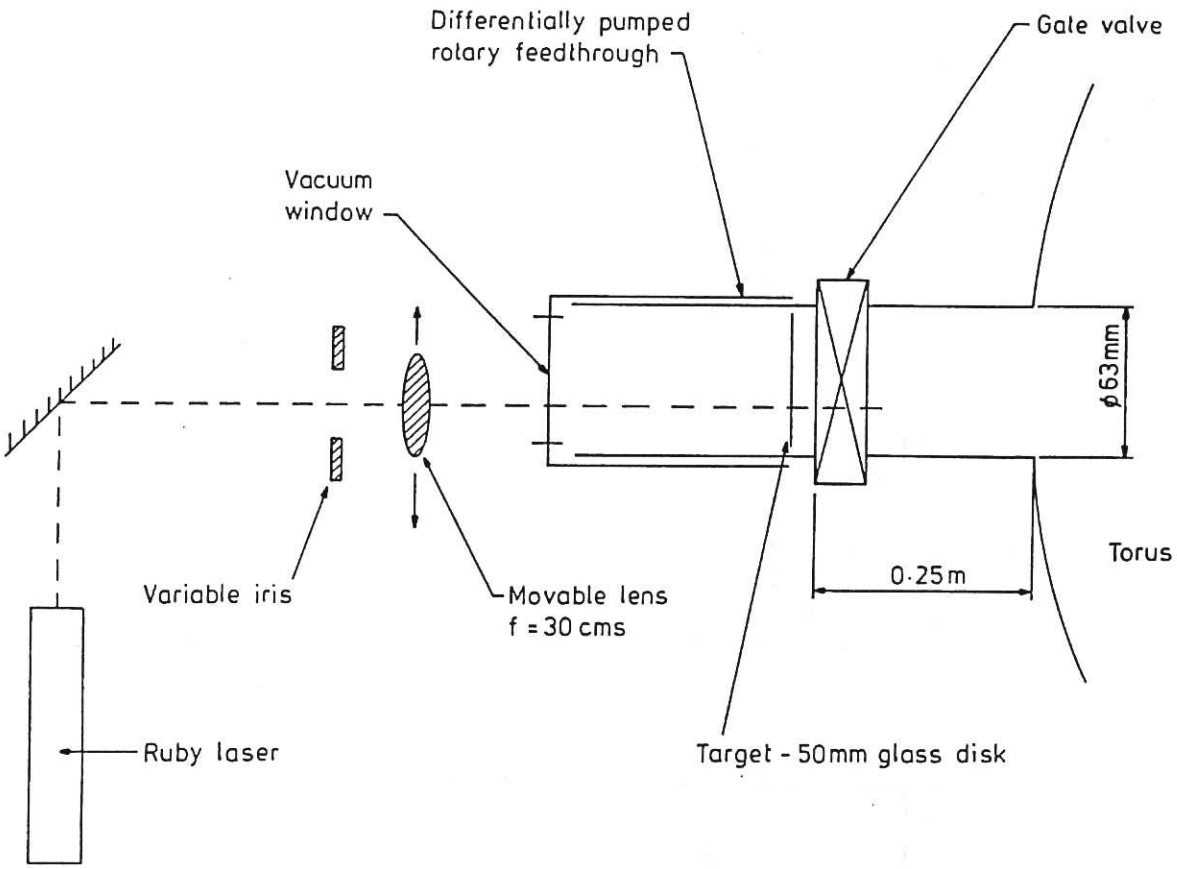

1 Laser ablation apparatus .

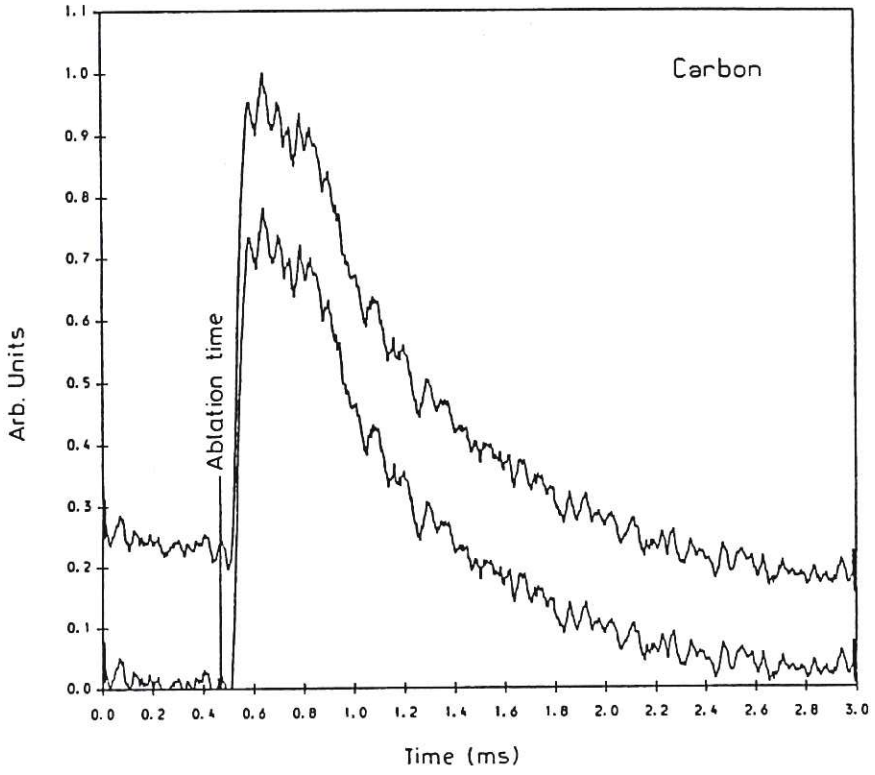

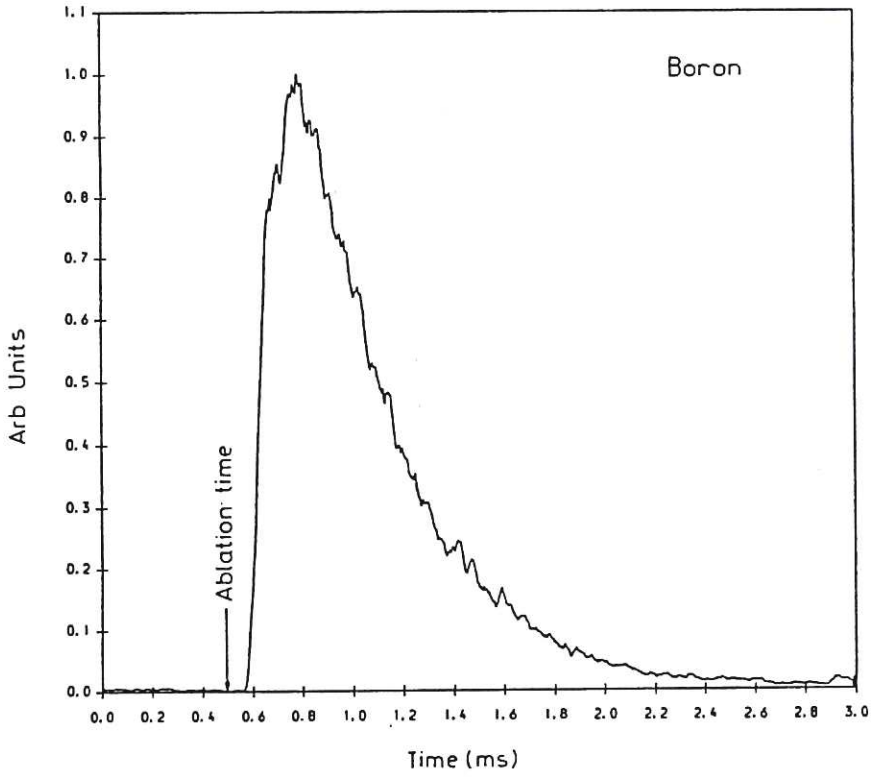

2 Temporal behaviour of carbon and boron preceding and following laser ablation. Note in the case of carbon, the lower trace has the background pedestal subtracted.

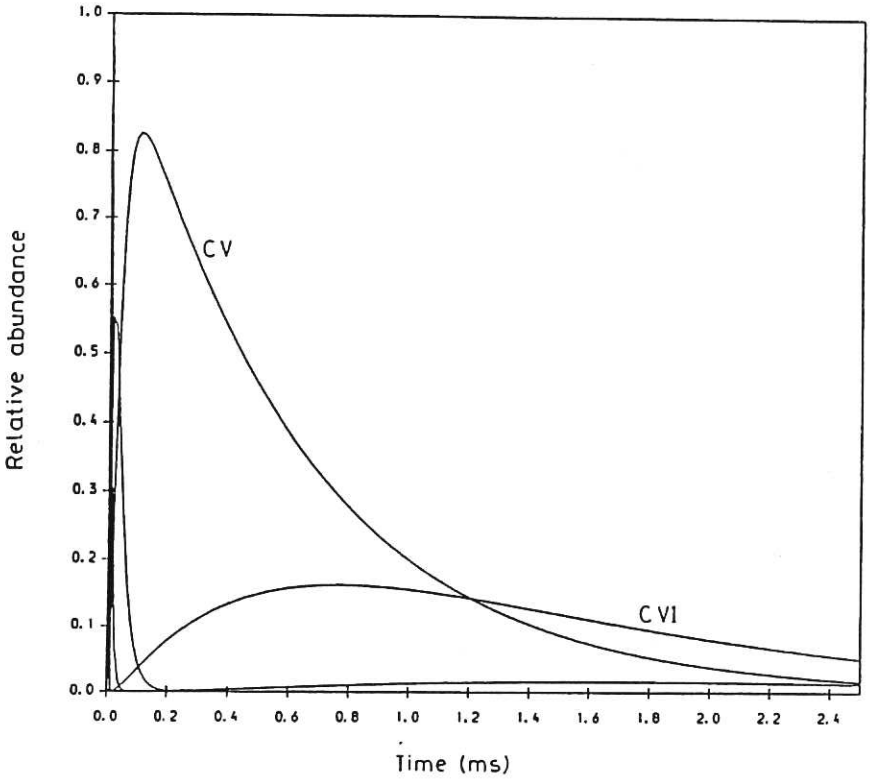

3 Calculated evolution of different states of carbon with time for a τ_p of 1ms.

CLM-P889

CLM-P889

10kW CO_2 Laser Welding of a High Yield Strength Steel

M. Hill
J. H. P. C. Megaw
A. Aitchison
J. H. Aubrey

CULHAM LABORATORY

AEA TECHNOLOGY

CLM-P889

10kW CO_2 Laser Welding of a High Yield Strength Steel

M.Hill, AEA Technology
J.H.P.C. Megaw, B.Sc., Ph.D., M.Inst.P., AEA Technology
A. Aitchison, Sen.M.Weld.Inst., Vickers Shipbuilding & Engineering Ltd.
J.H. Aubrey, B.Sc.,C.Eng.,M.I.Mech.E., Vickers Shipbuilding & Engineering Ltd.

To be published in the proceeding of the Second International Conference on Power Beam Technology - Laser and Electron Beam Processes, Stratford-upon-Avon, 23-26th September 1990.

10kW CO_2 Laser Welding of a High Yield Strength Steel

M.Hill,	AEA Technology
J.H.P.C. Megaw, B.Sc., Ph.D., M.Inst.P.,	AEA Technology
A. Aitchison, Sen.M.Weld.Inst.,	Vickers Shipbuilding & Engineering Ltd.
J.H. Aubrey, B.Sc.,C.Eng.,M.I.Mech.E.,	Vickers Shipbuilding & Engineering Ltd.

SUMMARY

This paper describes an investigation of 10kW CO_2 laser welding undertaken during BRITE Project 1206, where a major objective was to demonstrate automatic welding of large steel components with commercial edge preparations. A brief description of the overall project and some of the features of a 6m-stroke welding gantry are presented, together with a detailed account of the moving welding head equipment. The experimental procedure, where several different fillers were added to single-pass welds in 12mm thick Type Q1N steel plate, is described. Results of macro and micro-examinations, hardness measurements and Charpy impact tests show that welds with encouraging properties were produced.

INTRODUCTION

A three year European research and development project, BRITE P1206 - Adaptive Control of Laser Processing (1), on industrial applications of high power lasers for cutting, welding and surface treatment of metals was completed successfully in September 1989. A partnership of over twenty organisations, ranging from small and medium sized enterprises to large multi-nationals, from the Netherlands, West Germany and the United Kingdom sponsored the Project. Companies from a variety of industries, including several involved in shipbuilding and off-shore activities, were represented. Whilst the TNO Applied-Physics and Metals Institutes in the Netherlands used 300W Nd:YAG and 1.2kW CO_2 lasers to develop techniques for cutting, hardening, micro-machining (2) and surface texturing of metals utilised in the production of moulds for manufacturing plastic components, the Laser Technology Centre at Culham Laboratory studied the application of multikilowatt CO_2 lasers. A major objective was to design and construct a large-scale gantry to demonstrate adaptive control of welding with a 10kW CO_2 laser. Ultimately, the goal was the implementation of an automatic welding process on a moving welding system capable of operating continuously and over long distances. That necessitated studying various aspects of laser welding, in particular those affecting the welding process in thick-section steels, e.g. welding high strength materials and multi-pass welding. For some of the investigations a high yield strength quenched and tempered steel, Type Q1N, which is of particular interest in warship construction, was chosen in 12 and 25mm thicknesses. A further objective was to develop laser welding techniques suitable for use with commercial plate preparation, i.e. consistent with either readily machinable edge profiles or, if possible, flame cut edges.

Early developments at Culham using a 5kW CO_2 laser to weld guillotined and laser cut edges in 6mm mild steel plate with the addition of filler wire were very encouraging (3) and the potential for exploiting this technique in shipbuilding has been described (4). Similarly, the potential for joining heavier sections, such as off-shore pipeline, with a 10kW CO_2 laser using a moving welding head has also been demonstrated (5). Therefore, development of a fully automated laser welding process, with adaptive control of height following, seam tracking and joint gap filling, appeared to be a logical next step when formulating this BRITE project. Although the project was conducted

on a confidential basis, it is possible to report here some of the less commercially sensitive aspects and an account of the investigation into single-pass welding of 12mm thick Type Q1N steel plate with filler wire addition is presented.

EQUIPMENT

Welded specimens were produced with the 10kW CO_2 laser CL10 on the BRITE P1206 6m-stroke welding gantry, shown in Fig. 1. Figure 2 shows schematically the 12-18m flight path, where the beam (6) is transmitted via seven plane mirrors through a height changer and servo alignment mechanism to the welding head which contains a further two plane mirrors and an off-axis aspheric ~f/12.5 focusing mirror, as shown in Fig. 3. The complete welding head is mounted on a vertical slideway and transported on the gantry carriage. Figure 4 shows the travelling 10kW CO_2 laser welding head producing a bead-on-plate melt run in 12mm mild steel during open-loop trials. Much of the optical system was designed, tested and assembled during the first two years of the project (7).

Welding was performed in the downhand attitude in pairs of plates held horizontally and clamped together on a table designed to carry test specimens up to 6m long. Plasma control and protection against oxidation of the top surface was provided by means of a Culham standard gas shield (3), within which a 2mm diameter jet of inert gas is directed at an angle of 45° 1mm ahead of the laser beam/workpiece interaction point (Fig. 3). Filler wire, fed from an NEI/TWI Whiz-step wire feeder, was directed at ~60° to the plate surface to a position ~2mm ahead of the interaction point through three guide rollers. This auxiliary wire-feed mechanism, also developed during the project (7), proved very effective in straightening the wire and stabilising its pointing direction. Although not utilised for the work reported here, the welding head incorporated an Oldelft Seampilot vision system capable of sensing the transverse position, height and size of the joint gap and of providing feedback control to the motors which determine weld head position and wire feed rate.

MATERIALS

Type Q1N plate was supplied and prepared for the laser gantry welding trials by VSEL. Specimens ~300mm long by ~150mm wide were flame cut from 12mm thick plates; some of the specimens were machined along one edge either normal to the plate surface to provide a square-butt fit-up or at 5° from normal to give a 2mm wide V-preparation between pairs of close butted plates. The latter preparation was chosen to maintain sufficiently wide gaps to accept ~1mm diameter wires and to allow adequate penetration of filler materials throughout the plate thickness. All of the plates were descaled by sand blasting, oiled to prevent rusting during storage and then cleaned with Genklene before welding. An average of chemical analyses from four plate samples is given in Table 1.

Five different types of welding wire were used. Initial trials were made with a double de-oxidised MIG welding wire, DIN8559-SG2, originally specified for a shipbuilding application and used successfully in the second year of this project for double-pass welding in 25mm material (1). Another double and a triple de-oxidised wire to BS2201, Part 1-A18 and A15 respectively, were employed: A18, because it is more readily available than SG2; A15 for possible use with flame cut edges. Linde 95 wire was chosen because it is used in arc welding Q1N plate to give high strength and toughness. Since flux cored wires have shown considerable improvements in laser weld metal microstructures and Charpy impact energies at low temperature (8) (9), a wire of this type, Dual Shield II-101TM was also tried. The L95 and DSII were supplied by VSEL and specimens from all five wires were arc melted under argon shielding and chemically analysed by VSEL, with the results shown in Table 1.

Table 1 Chemical analyses of plate and fillers (%Wt)

Element	Average Q1N Plate	Filler				
		SG2	A18	A15	L95	DSII
C	0.14	0.06	0.04	0.035	0.07	0.05
Mn	0.29	1.35	1.29	1.07	1.68	1.10
P	0.012	0.015	0.015	0.013	0.008	0.006
S	<0.002	0.012	0.017	0.005	0.006	-
Si	0.25	0.68	0.78	0.55	0.33	0.33
Ni	2.88	0.074	0.09	0.055	1.66	1.66
Cr	1.35	0.014	0.06	<0.01	0.1	0.02
Mo	0.37	0.01	0.006	0.015	0.31	0.01
Ti	0.006	0.005	0.004	0.080	0.01	-
V	0.007	0.006	0.006	0.009	<0.01	0.02
Cu	0.016	0.53	0.27	0.20	0.02	0.01
Co	0.011	0.007	0.013	0.013	-	-
As	0.007	0.004	-	-	-	-
Sb	<0.005	<0.005	-	-	-	-
Pb	<0.002	<0.003	-	-	-	-
Sn	0.002	0.004	-	-	-	-
Al	0.026	<0.002	<0.005	0.045	0.02	-

EXPERIMENTAL PROCEDURE

During the first two years of the project a wide ranging parametric study on keyhole phenomena was made using off-line radiography and on-line, real time radiography. The study showed that fully penetrating welds, with low levels of porosity, could be produced in 12mm mild steel with a power ~8kW at the work and welding speed ~10mms^{-1}, when focusing the CL10 beam with off-axis spherical mirrors between f/8 and f/16. Therefore for the gantry welding trials a 500mm focal length mirror, equivalent to ~f/12.5, was used with a power of 7.5 ±0.2kW at the work. Initially, a series of bead-on-plate melt runs were made and the focus position was chosen to be 2mm below the top surface of the plate, for which condition maximum penetration was obtained for a given power and speed. Helium was used throughout for plasma control and shielding; jet, lens and top shroud flow rates were 15,50 and 50 lmin^{-1} respectively. Those were the optimum values found for the bead-on-plate runs and they also proved to be very effective when welding with filler.

An investigation was then performed to find suitable combinations of welding speeds (S) and filler wire feed rates (R) to fill the 2mm Vee joint gap. As a starting point the ratio of wire feed to welding speed was assumed to be equal to the ratio of joint gap area (A) to wire cross-sectional area (a). Thus:

$$\frac{R}{S} = \frac{A}{a} = \frac{0.5\ wt}{\pi r^2}$$

where (w) is the Vee top width, (t) plate thickness and (r) wire radius. Allowing for shrinkage (δ) and angular 'butterfly' distortion (α) during welding, A is reduced so that:

$$\frac{R}{S} \approx \frac{(0.5w - \delta - 0.5t\ \tan\alpha)t}{\pi r^2}$$

Therefore, for t=12mm, w=2mm, r=0.5mm and assuming δ ~0.25mm and α ~1° (as measured in previous CL10 welding with filler): R/S ≈ 9.9. In practice, when welding with the 1.0mm diameter SG2 wire a fully penetrating weld was produced with good joint gap filling by using a welding speed of 8mms^{-1} and wire feed rate of 80mms^{-1}. Therefore, 1.0mm diameter A15 and A18 wires were used with the same speeds and produced similar results. A feed rate of 95mms^{-1} for 0.95mm diameter L95 wire produced a good result at the same welding speed, giving R/S ≈ 12 compared to the 10.9 calculated. For 1.2mm O.D. DSII wire, weld and wire speeds of 8mms^{-1} and 80mms^{-1} respectively gave an acceptable result.

Two attempts were made to feed 1.0mm diameter A15 wire at 50 and 25mms^{-1} into joints between flame cut plates with an 8mms^{-1} welding speed. Both attempts failed due to the wire not entering the narrow joint (<1mm wide) and deflecting out of the molten region, thus producing two autogenous welds. Two further autogenous welds were produced at 6 and 12mms^{-1} in close butted joints with machined edges for metallurgical comparison of welding with high and low heat input, i.e. nominally 1.25 and 0.63kJmm^{-1} respectively.

RESULTS

Visual examination of the underside of the welded plates showed full penetration and generous under beads in all welds except for the high speed (12mms^{-1}) autogenous weld which had only partial penetration. Top beads were smooth and indicated adequate filling in most welds. Those welded with A18 and DSII fillers were slightly under-filled. The autogenous welds in flame cut edges were also under-filled, with slightly disrupted top beads. Photomacrographs of sections from each of the welds are shown in Fig. 5. Satisfactory weld bead profiles and good side-wall fusion are seen for all of the welds with filler, but the autogenous welds are rather barrel shaped and therefore not ideal. Micro-porosity near the fusion boundary is seen only in the welds with A18, A15 and L95 fillers.

Hardness measurements were made with a Vickers diamond point hardness tester using a 10kg load at various positions across the weld beads and in the heat affected zones (HAZ) and parent plate on either side of the welds. Tests were made at three positions within the plate thickness, i.e. 1.5mm from the top and bottom surfaces and at the plate centre. Average on-axis well hardnesses range as follows: SG2, 373HV_{10}; DSII, 379HV_{10}; A15, 385HV_{10}; 12mms^{-1} autogenous 391HV_{10}; 6mms^{-1} autogenous, 392HV_{10}; A18, 395HV_{10}; L95, 404HV_{10}; flame cut edges, 408HV_{10}. Hardness varies across the HAZ: in the lightly etched regions close to the fusion boundary (see Fig. 5) hardnesses are comparable with, or sometimes a little higher than those on the weld axis, with a maximum value of 425HV_{10} near the top of the HAZ of the L95 filler weld; in the outer HAZ regions typical values are generally below 300HV_{10}, whilst the average parent plate hardness is 223HV_{10}. These values should be noted in the context of VSEL's maximum acceptance value of 350HV_{10}.

Charpy impact toughness tests were made in 10mm x 10mm specimens machined from each welded plate, with the V-notch running from top to bottom of the weld bead and its centre placed on the weld axis, i.e. running vertically in the sections shown in Fig. 5. Tests were made at temperature intervals of 10°C from 0°C to -70°C for each weld. The measured impact energies where specimens broke along the weld centre line are plotted in Fig. 6; values usually >200J, where the fracture deviated into the parent plate, were ignored. The graphs show that two of the filler wires, SG2 and DSII, produced average Charpy values greater than the VSEL average acceptance value of 85J at -50°C. The values for double and triple de-oxidised wires (A18 and A15) were slightly below that requirement, although they were higher than the minimum acceptance value of 50J. Results for L95 were considerably lower than expected, surprisingly so since this wire gives excellent impact properties (80-95J at -50°C) with conventional arc welding.

Autogenous welding of machined edges appears to be fairly satisfactory, giving almost exactly the required average Charpy value. However, the flame cut edges when welded without filler gave less than half that value, presumably reflecting effects due to heavily oxidised edges.

Optical microscopy shows that generally the weld metal microstructures consist of coarse columnar untempered martensite near the weld crown, becoming slightly more equiaxed with weld depth. No acicular ferrite was observed, although the sub-grain microstructure of the DSII filler weld metal is considerably finer than any of the other welds. This is shown in Fig.7 in comparison with the SG2 filler weld metal. Close to the fusion boundary, the heat affected zone consists of coarse equiaxed grains of untempered martensite; this structure becomes increasingly tempered and fine grained as the fully-tempered martensite of the parent plate is approached.

CONCLUSIONS

Following completion of the design, construction and commissioning of the 6m gantry during the first two years of the project, it was possible to demonstrate successfully single-pass welding of 12mm thick Type Q1N steel plate by means of a moving 10kW CO_2 laser welding head and with the addition of various filler wires. Choice of a 2mm wide V-preparation enabled full-depth penetration of the filler materials, which produced sound weld bead profiles having good side-wall fusion, minimal slumping and smooth top and bottom beads. Small amounts of microporosity were seen in only a few of the welds. Weld shrinkage and butterfly distortion were low (~ 0.25mm and ~ 1°) and consistent, thus allowing wire feed rates to be predicted accurately.

Addition of a particular double-deoxidised MIG welding wire, DIN8559-SG2, and a rutile flux cored wire, Dualshield II, produced low temperature Charpy impact energies satisfying the appropriate welding acceptance values for this material. However use of the TiO_2-containing flux-cored wire did not produce acicular ferrite as had been observed in previous laser welding of a pressure vessel steel (9). Charpy results for welds made with another double and a triple de-oxidised wire, A18 and A15, approached the average acceptance value, but those produced with a filler suitable for arc welding Q1N plate, Linde 95, were below that value. The autogenous welding of heavily oxidised flame cut edges resulted in greatly reduced impact energy, but the autogenous welding of machined edges at $6mms^{-1}$ gave impact values comparable to some obtained in filler welding. Testing of the lower heat input ($12mms^{-1}$) autogenous welds yielded more fracture deviation. It is also noted that there appears to be some correlation between the impact properties shown in Fig. 6 and the weld hardness noted above, i.e. the better Charpy performance of the SG2 and DSII fillers corresponds to weld hardness $<380HV_{10}$, whilst the poorer impact properties of the welds using L95 filler or flame cut edges correspond to weld hardness $>400HV_{10}$.

An attempt has been made to compare the present results with those from other work (10) on the autogenous laser welding of two casts of Q1N plate. Simple comparisons are rendered difficult by the ubiquitous problem of crack deviation, but it may be inferred that the present autogenous results indicate higher impact energies. This is difficult to explain on the basis of carbon content because it is here comparable with that of the preferred cast in the other work; on the other hand, sulphur levels in the present work are lower (<0.002% cf 0.003%).

In summary, notwithstanding the rather high hardness of the joint region in the as-welded condition, the measured impact properties are generally better than might be expected, given the growing body of data which suggests that laser weld toughness is an area requiring special attention.

ACKNOWLEDGEMENTS

We wish to thank the staff from the Laser Technology Centre and ACAP Group at Culham Laboratory who developed the 6m gantry system and assisted in producing the welded plates and those from VSEL's Metallurgical Laboratory where the weld analysis was undertaken. Technical and financial support is also gratefully acknowledged from the CEC-DGXII and the following BRITE P1206 Partners and Sponsors: AGA Gas, General Electric Plastics, TNO, Oldelft, Philips Research, and Van Leer from the Netherlands; Heraeus Industrielaser, Interatom and Trumpf from West Germany; and British Aerospace, British Maritime Technology, British Shipbuilders, Ferranti, GKN Technology, Harland and Wolff, Integrated Laser Systems, NEI Parsons, Rolls-Royce, Shell Research, Swan Hunter and The Welding Institute from the UK.

REFERENCES

1. Spalding IJ: Adaptive control of laser processing - BRITE P1206, BRITE/EURAM 2nd Technological Days, Brussels, February 1989.
2. Van Krieken AH, Groote Schaarsberg J, and Raterink HJ: Laser micro-machining of material surfaces, 34/SPIE, Vol. 1022, Laser Assisted Processes, Hamburg, September 1988.
3. Megaw JHPC, Hill M and Johnson R: Laser welding of steel plates with unmachined edges, Proc. Conf. Inst. of Metallurgists, Joining of Metals - Practice and Performance, Warwick, April 1981.
4. Martyr DR: The application of high power laser technology to ship production, N.E. Coast Inst. of Eng. and Shipbuilding General Meeting, Newcastle-upon-Tyne, February 1985.
5. Megaw JHPC, Hill M and Osbourn SJ: Girth welding of X-60 pipeline with a 10kW laser, Proc. SPIE/ANRT Conf. on High Power Lasers and Their Industrial Applications, Innsbruck, April 1986.
6. Spalding IJ, Selden AC, Hill M, Megaw JHPC and Ward BA: High power CO_2 lasers, 7th Int. Symp. on Gas Flow and Chemical Lasers, Vienna, August 1988.
7. Ward BA, et al: The design of a 6 metre laser welding gantry,
BRITE Project 1206 Report, CLM/RR/BRITE/T7/1, December 1989.
8. Hakansson K: High power laser beam welding of different steels, Joining of Metals - 2, Helsinger, April 1984.
9. Stares IJ, Apps RL, Megaw JHPC, and Spurrier J: Improved microstructure and impact toughness of laser welds in a pressure vessel steel, Metal Construction, 19(3), 123-126, March 1987.
10. Galsworthy JC and Oakley PJ: An assessment of the laser welding of 12mm thick quenched and tempered steel plate, Int. Conf. on Advances in Joining and Cutting Processes, Harrogate, October 1989.

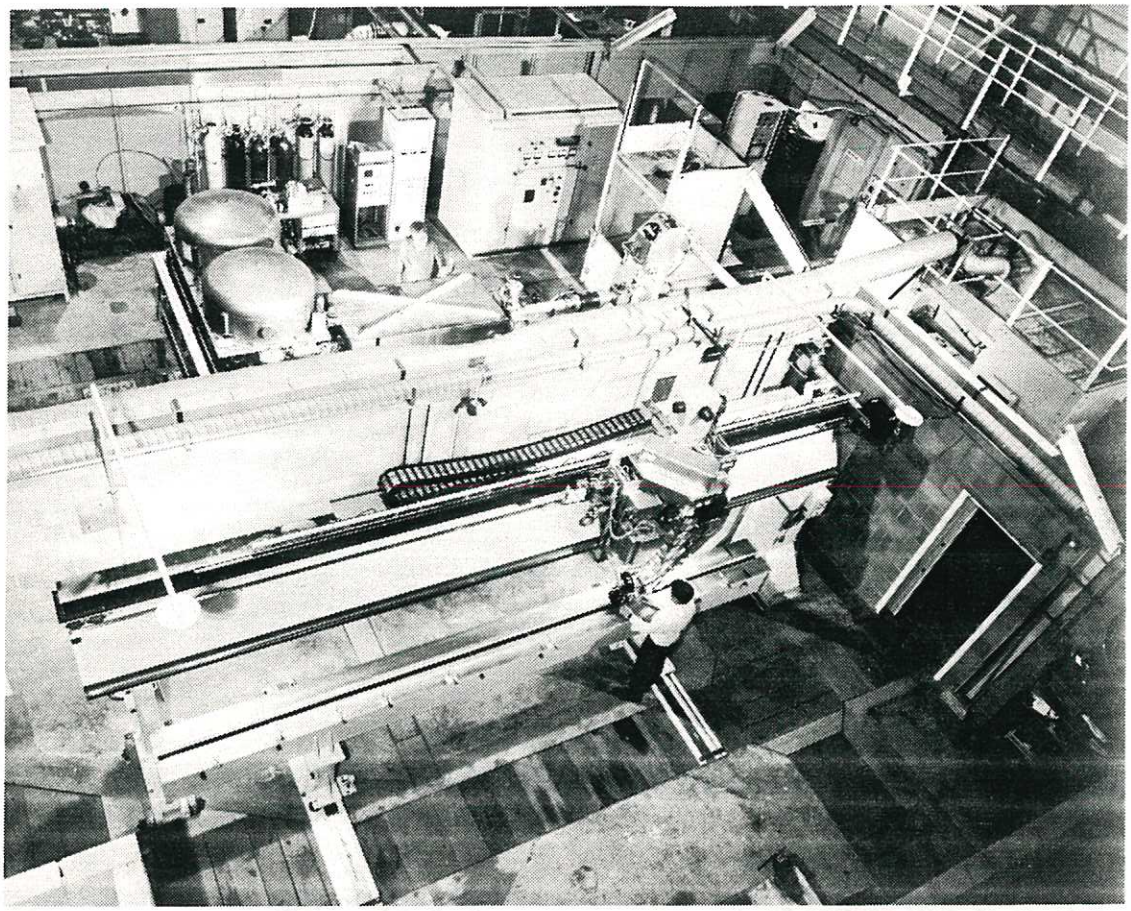

Figure 1. Overhead view of the 10kW CO_2 laser and the 6m welding gantry.

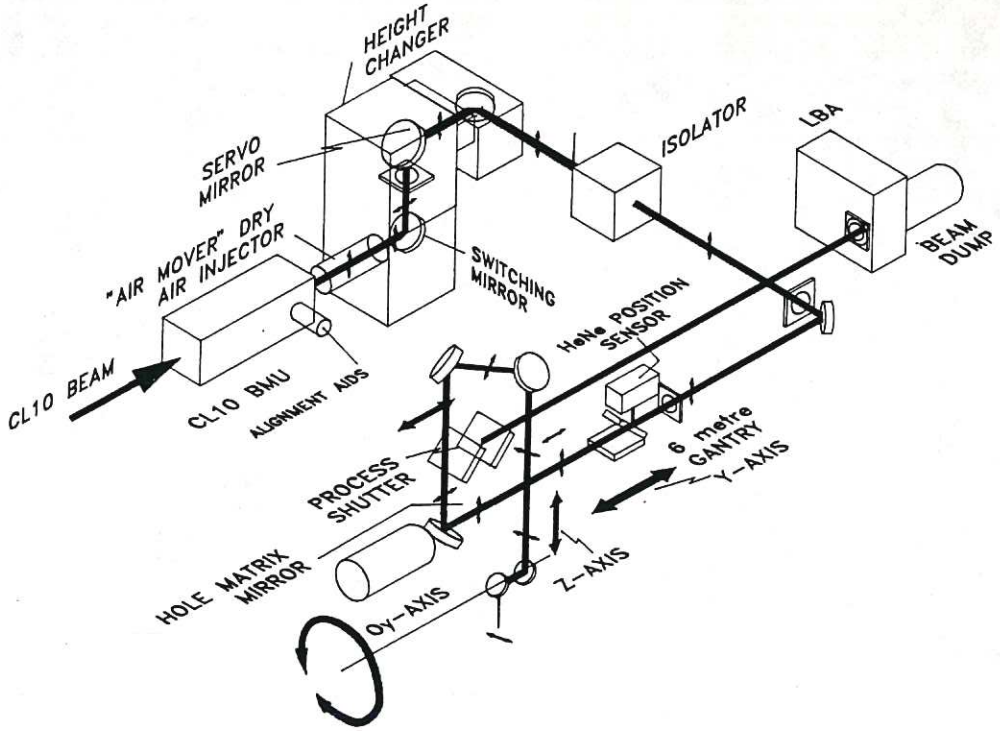

Figure 2. Optical schematic of the gantry system.

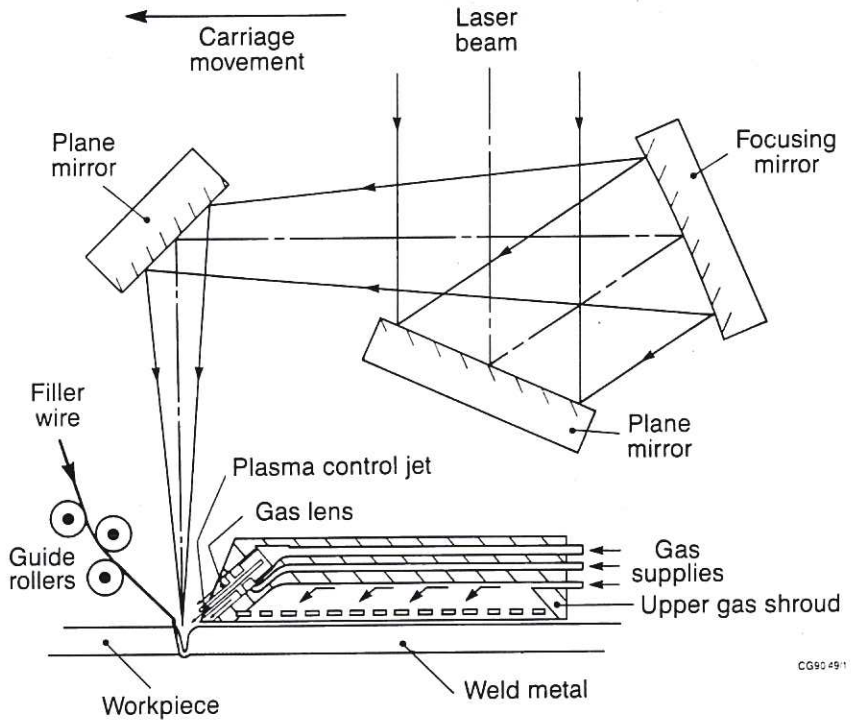

Figure 3. Laser welding head and wire feed schematic.

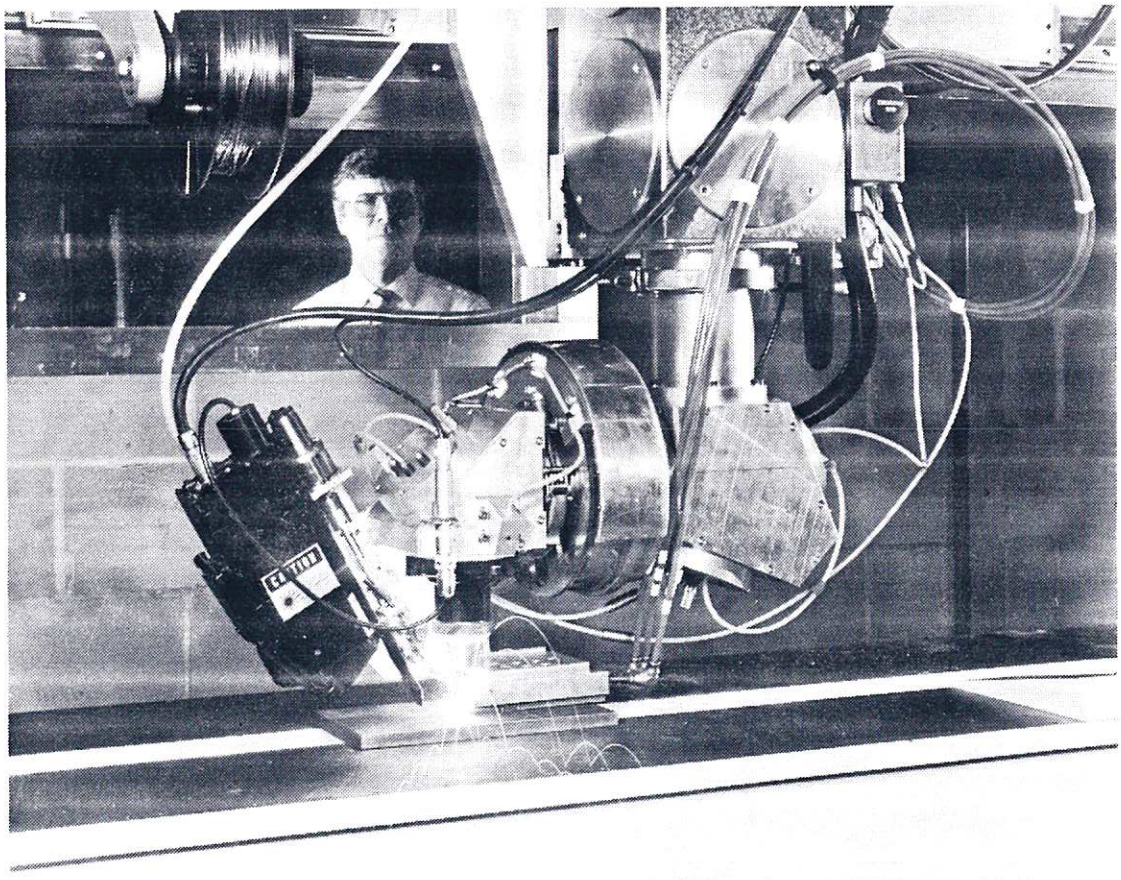

Figure 4. View of the laser welding head making a bead-on-plate run in 12mm mild steel on the 6m gantry.

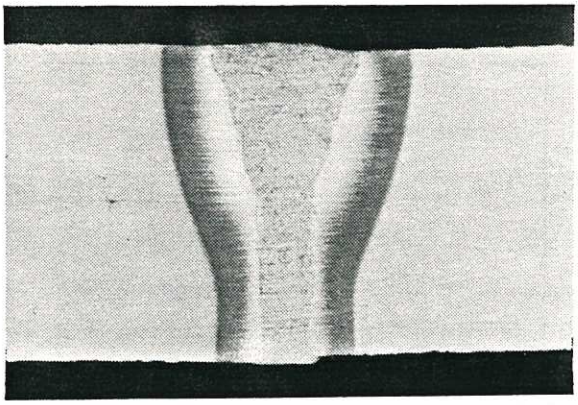

SG2 Wire 8mms^{-1}

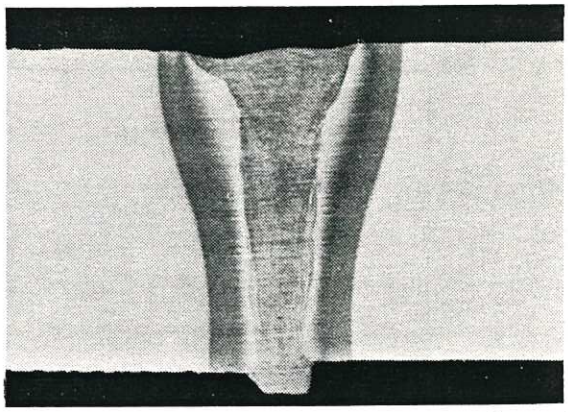

Dualshield II Wire 8mms^{-1}

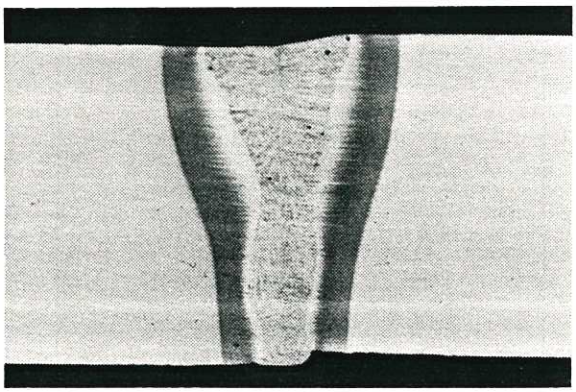

A18 Wire 8mms^{-1}

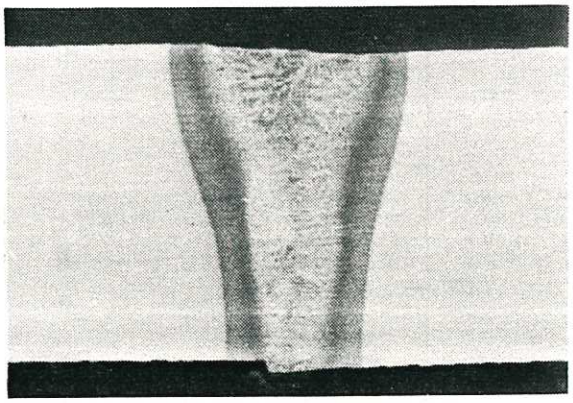

Flame Cut 8mms^{-1}

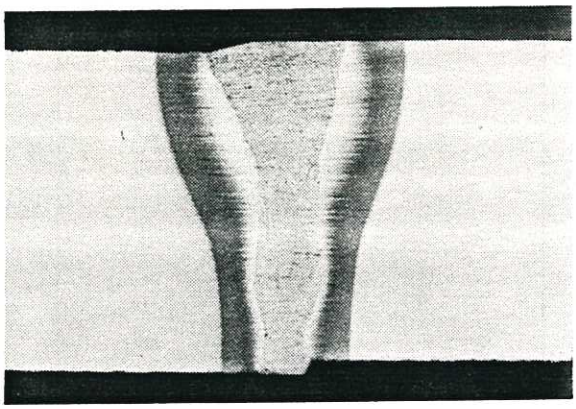

A15 Wire 8mms^{-1}

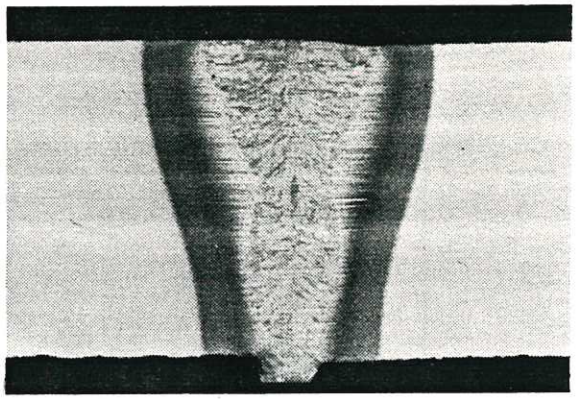

Autogenous 6mms^{-1}

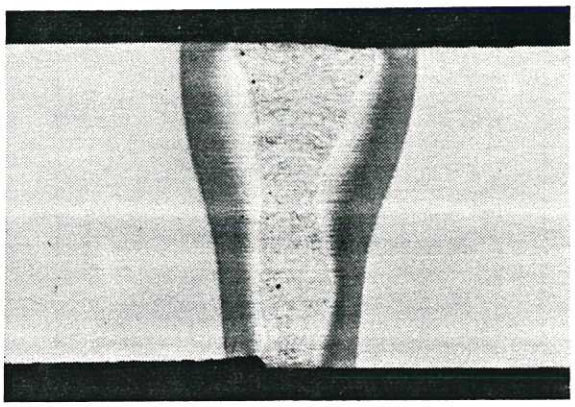

Linde 95 Wire 8mms^{-1}

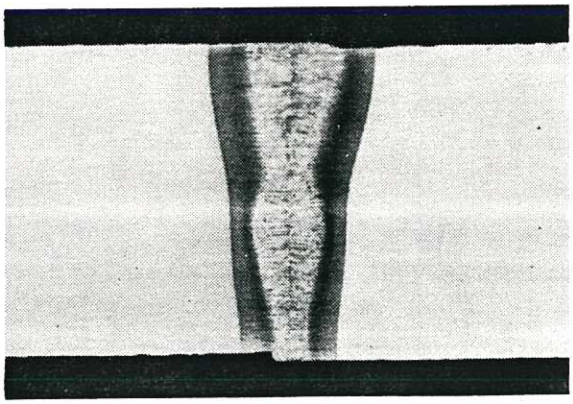

Autogenous 12mms^{-1}

Figure 5. Macro-sections from laser welds in 12mm thick Type Q1N steel plate.

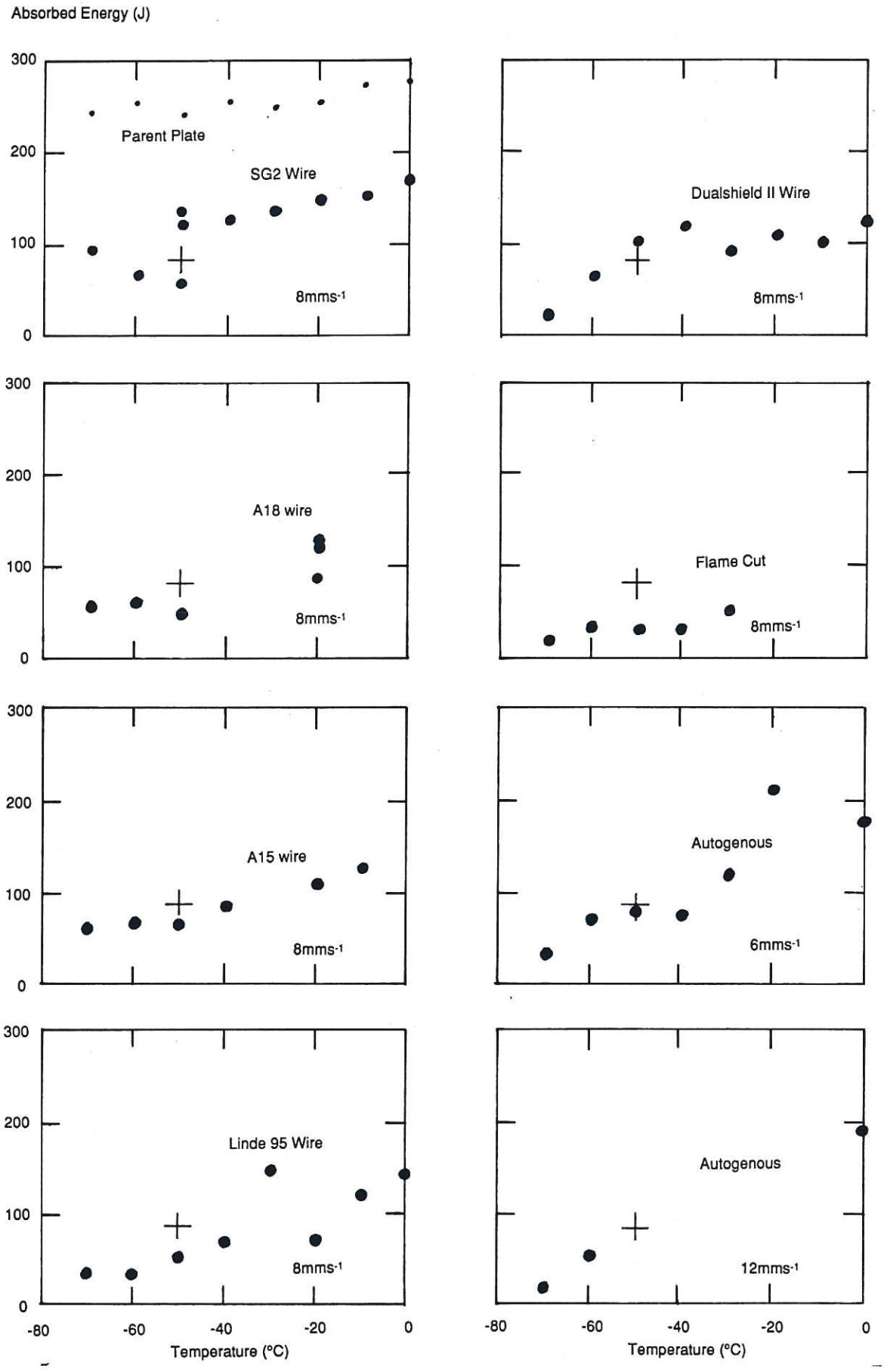

Figure 6. Charpy absorbed energies in laser welded Type Q1N plate: 7.5kW at work; + denotes VSEL average acceptance value.

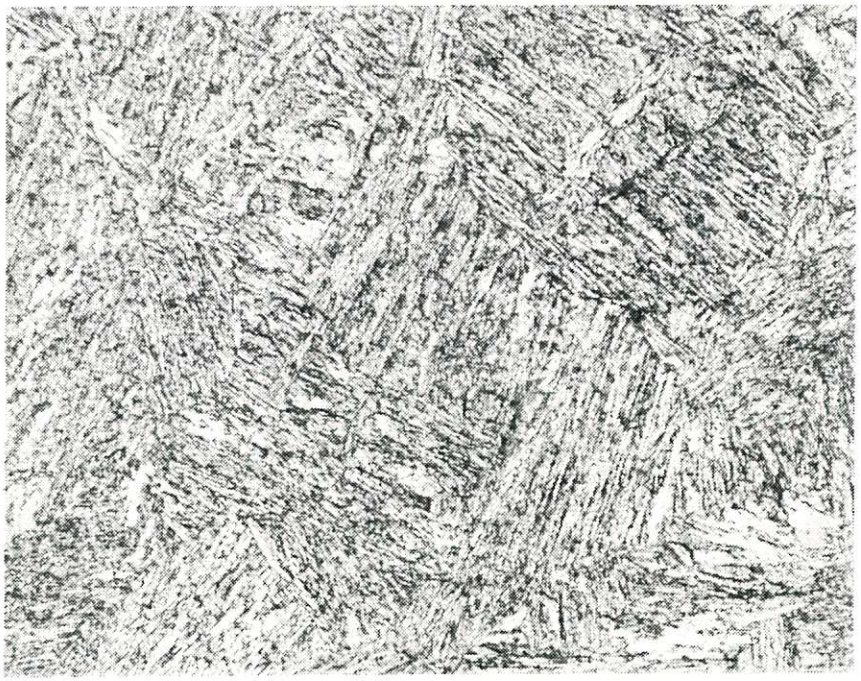

20μm

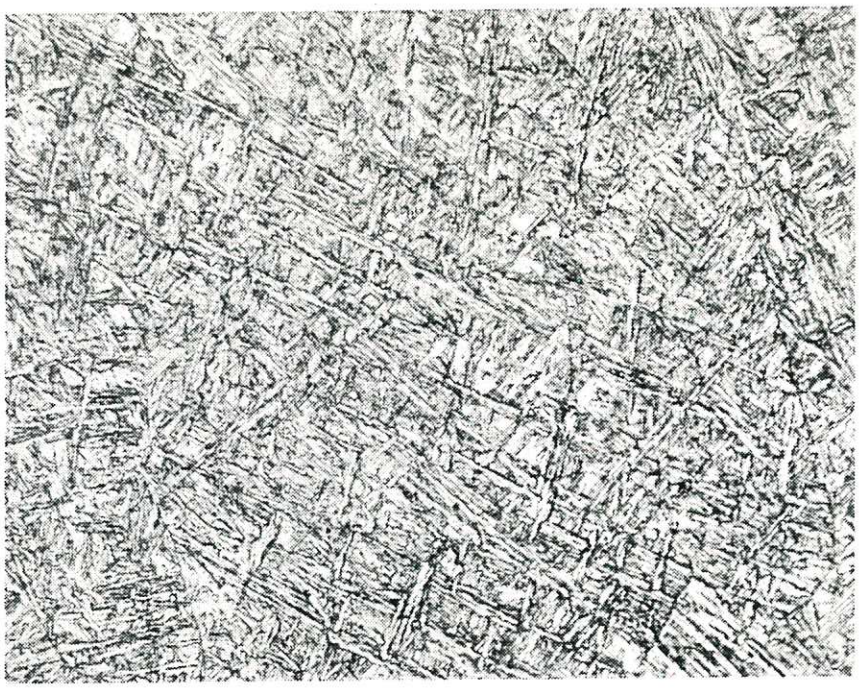

Figure 7. Weld metal microstructures from SG2 (upper) and DSII (lower) filler welds.